

pubs.acs.org/journal/ascecg Research Article

# Antibacterial Nanofibrous Mat of Pullulan/Cinnamaldehyde-Cyclodextrin Inclusion Complexes as a Potential Cloth Mask Layer with Long-Term Storage Stability and Facile Disposal Property

Asli Celebioglu, Christopher W. Lawson, Emmy Zhiren Hsiung, Rimi Chowdhury, Craig Altier, and Tamer Uyar\*



**Cite This:** ACS Sustainable Chem. Eng. 2023, 11, 11269–11280



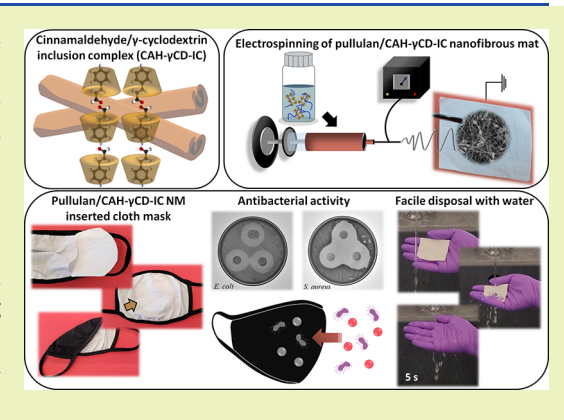
**ACCESS** I

III Metrics & More

Article Recommendations

s Supporting Information

ABSTRACT: There is an ongoing rise in global plastic waste because of the mass production and vast consumption of surgical face masks during the COVID-19 outbreak. This problem leads to a crucial need for alternative face coverings which can eliminate environmental concerns. Using cloth masks can be a sustainable solution if combined with a functional filtering layer. In this study, electrospun nanofibrous mats (NM) were generated using a renewable biopolymer; pullulan by the incorporation of cyclodextrin inclusion complexes (γCD-IC) of naturally occurring essential oil compound; *trans*-cinnamaldehyde (CAH). Pullulan/CAH-γCD-IC NM was readily inserted into a cloth mask due to its free-standing and foldable features and achieved higher loading efficiency ( $\sim$ 62%) than pullulan/CAH NM ( $\sim$ 10%). Here, pullulan/CAH-γCD-IC NM showed substantial and better antibacterial activity, long-term storage stability, and thermal stability due to inclusion complexation. Pullulan/CAH-γCD-IC NM was also obtained with promising properties of pore size



(~390 nm) and water vapor permeability (~890 g/m<sup>2</sup>/day). The water solubility of pullulan/CAH- $\gamma$ CD-IC NM ensured fast and easy disposal without potential environmental loading, thanks to the biocompatibility of components. Briefly, pullulan/CAH- $\gamma$ CD-IC NM can create an attractive alternative as a functional layer that can be combined with the cloth mask.

KEYWORDS: electrospinning, nanofibers, cyclodextrin, pullulan, cinnamaldehyde, essential oil, antibacterial, face mask

## ■ INTRODUCTION

The global epidemic of COVID-19 has infected more than 760 million and killed over 6.9 million people by the end of April 2023. This difficult duration has shown that protection of the respiratory system is the easiest and most reliable method to avoid the spreading of infection.<sup>2</sup> The use of surgical face masks is still considered one of the most effective ways to prevent penetration of viruses, bacteria, or pathogens into the human body.<sup>2,3</sup> Therefore, COVID-19 outbreak has significantly boosted the manufacturing and consumption of surgical face masks. However, the intensive use of these masks having neither reusability nor antimicrobial property has caused a critical level of worldwide pollution because of increasing plastic waste in the environment.<sup>4</sup> Additionally, discarded surgical face masks thereafter usage has caused an increased risk of secondary virus transmission and another loading to the environment with a requirement of safe disposal.5 The disinfection processes have been applied for the contaminated surgical face masks to overcome their reusability issue; however, this has resulted in a decline in their filtering performance because of the damaged structure.<sup>6</sup> The filtering layers of the face mask have been also incorporated with

metals/inorganic materials including copper, silver, zinc, and titanium dioxide to attain antimicrobial and antiviral properties. However, there has been a growing concern about their application because of their potential risks to the human health and ecosystems. Unfortunately, all these efforts made to increase the reusability of surgical face masks have remained incapable to overcome the aggravated problem of global plastic waste. Because the nonwoven layers of surgical face masks are produced using polymers such as polypropylene (PP), polystyrene (PS), and polyacrylonitrile (PAN) which can persist in the environment for centuries. Meanwhile, these polymeric layers can decompose and degrade into micro- and/ or nano-plastics as another ecotoxicological threat for the environment. Between the surgical surgical

Received: May 3, 2023 Revised: June 30, 2023 Published: July 18, 2023





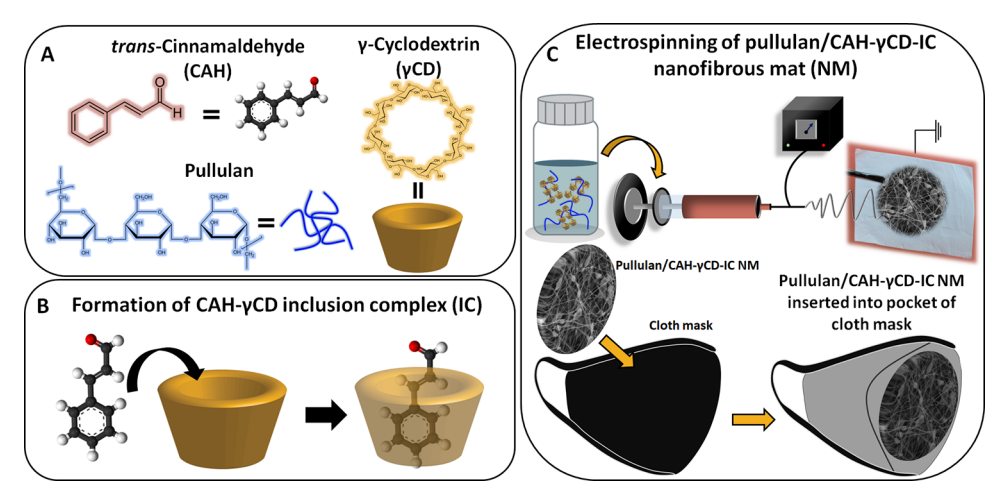


Figure 1. (A) Chemical structure of CAH,  $\gamma$ CD and pullulan. (B) Schematic representation of inclusion complex (IC) formation between  $\gamma$ CD and CAH. (C) Schematic representation of the electrospinning of pullulan/CAH- $\gamma$ CD-IC nanofibrous mats (NM) and the insertion of pullulan/CAH- $\gamma$ CD-IC NM into a cloth mask pocket.

On the other hand, it has been shown that cloth masks ensuring better breathability and wearing comfort compared to surgical face masks can be effective to a certain extent in inhibiting the transition of droplets and aerosols that carry viruses. As expected, the filtration performance of cloth masks is not as effective as surgical masks and it highly depends on different variables such as fiber types (cotton, silk, nylon, polyester, polyurethane, etc.), fabric types, layer number, and/ or thread counts.<sup>9,10</sup> Wearing cloth masks can be a sustainable solution from the point of environmental aspects; however, a filtering layer needs to be inserted into these masks to enhance and standardize their filtration performance. 11 Herein, electrospun nanofibrous mats have drawn great attention as a promising filtering material due to their attractive properties such as tunable porosity, ultra-thin fibrous structure, lightweight, diversity of used components, and modification convenience. 12

Recent studies have shown that nanofibrous mats generated using various biodegradable polymers such as ethyl cellulose, <sup>13</sup> polybutylene adipate terephthalate (PBAT),<sup>14</sup> poly(lactic acid) (PLA),<sup>15–18</sup> and polycaprolactone (PCL)<sup>19</sup> have high potential to be used as filtering layer for the face masks. Moreover, they can minimize the environmental footprints which can occur in case of non-biodegradable synthetic polymers. It is evident that a large part of these studies has focused on using PLA for this purpose due to its high potential for biodegradation. However, Soo et al. showed in one of their related studies that even PLA-derived face masks displayed a limited performance to overcome the plastic pollution problem of the pandemic since PLA degrades slowly and under specific conditions only. 20 At this point, water-soluble polymers which can be readily disposed of by a simple washing or dissolve in an aqueous medium can be an attractive alternative. There have been reported studies where the well-known water soluble polymers; polyvinyl alcohol (PVA),<sup>21</sup> and polyvinylpyrrolidone (PVP)<sup>22</sup> were used to generate a functional filtering layer in the form of a nanofibrous mat. However, a polymer type that is provided from a renewable source might be a more promising option compared to fossil-fuel based polymers to ensure sustainability and eliminate environmental concerns.

Pullulan is a microbial polysaccharide produced on an industrial scale by the fermentation of starch syrup.<sup>23</sup> It is an abundant type of water-soluble biopolymer that is widely used

in pharmaceutical, cosmetic, and food applications owing to its biocompatible, non-toxic, non-mutagenic, odorless, and edible properties.<sup>24</sup> Additionally, the linear macromolecular structure of pullulan enables the easy generation of mats and fibrous materials from this polymer. 23 Previous works of our group have also demonstrated that nanofibrous mats of pullulan can be successfully produced using electrospinning technique by the incorporation of various active compounds such as drug, antibacterial compounds,<sup>26</sup> and essential oil.<sup>27</sup> Due to ease of functionalization, a part of electrospun nanofibrous mats developed for the purpose of face mask application have been also incorporated with different additives including silver nanoparticles, <sup>13</sup> cetyltrimethylammonium bromide (CTAB), <sup>14</sup> zinc (oligo-lactate), <sup>15</sup> copper-based metal—organic framework (Cu-MOF), <sup>17</sup> zinc oxide nanoparticles, and <sup>19,21,22</sup> licorice root extract<sup>21</sup> to attain antibacterial or antiviral properties. On the other hand, essential oil compounds derived from plant sources can be an interesting alternative for the modification of electrospun nanofibrous mats that will be applied as functional filtering layers in the face masks due to attractive properties of essential oils such as antibacterial, fragrance, antifungal, antioxidant, and so forth.<sup>28</sup>

trans-Cinnamaldehyde (CAH) is the main essential oil compound found in the bark of cinnamon (85-90%) and responsible for the flavor and odor of this spice.<sup>29</sup> Moreover, it possesses a remarkable antimicrobial activity and can also inhibit the growth of yeasts, molds, and the production of toxins from these micro-organisms. Due to all these reasons, CAH has recently sparked the interest of both food and pharmacy industry as an antibacterial agent which is derived from a natural source and has been Generally Recognized as Safe (GRAS) by the United States Food and Drug Administration (FDA).<sup>29</sup> It is obvious that CAH can be also an attractive agent that will be used for the functionalization of the nanofibrous mat layer inserted into face masks, thanks to its pleasant odor, antibacterial activity, and further medicinal features. As most essential oil compounds, CAH also suffers from potential losses during processing and/or long-term storage because of its volatile nature and sensitivity to heat, light, and air.<sup>29</sup> The electrospinning technique represents a feasible way for the encapsulation of essential oils in the nanofibrous mat matrix; however, the single performance of polymeric templates may not be enough for the preservation of these volatile compounds.<sup>30,31</sup> Here, cyclodextrins (CDs), starch-derived cyclic oligosaccharides, can emerge as an effective encapsulation agent.<sup>32,33</sup> CDs display cost-effective and "green" solutions by enhancing the stability as well as solubility of volatile and hydrophobic essential oil compounds by forming inclusion complexes. 32,33 As it has been reported previously, the drawbacks of CAH molecules such as instability observed under ambient conditions and poor water solubility have been also overcome by inclusion complexation using different types of CDs. 32,34 The CD inclusion complexes have been used for the functionalization of cotton surfaces for antibacterial and/or antifungal applications. 35,36 In this study, the  $\gamma CD$  inclusion complexes of CAH molecules have been first incorporated into electrospun pullulan nanofibers (pullulan/CAH-γCD-IC NM) using a one-step process for developing a functional layer that can be inserted in the cloth mask (Figure 1). A comparative and detailed physical characterization has been performed with the control sample, CAH-loaded pullulan nanofibers (pullulan/CAH NM). The superior antibacterial activity and long-term stability of pullulan/CAH-γCD-IC NM compared to pullulan/CAH NM have been demonstrated, as well.

#### EXPERIMENTAL SECTION

**Materials.** Gamma cyclodextrin (γCD, Cavamax W8 Food) is a gift from Wacker Chemie AG (USA) for scientific studies. Pullulan  $(M_{\rm w}: 300,000~{\rm g/mol},~{\rm TCI}~{\rm America}),~{\it trans}\text{-cinnamaldehyde}$  (CAH, >98%, Thermo Scientific), deuterated dimethylsulfoxide  $(d_6\text{-DMSO}, 99.8\%,~{\rm Cambridge}~{\rm Isotope}),~{\rm and}~{\rm ethanol}~{\rm (absolute}~{\rm for}~{\rm analysis}~{\rm Emsure},~{\rm Sigma-Aldrich})~{\rm were}~{\rm provided}~{\rm commercially}.$  The chemicals were used without purification. High-quality distilled water was supplied from a Millipore Milli-Q ultrapure water system (Millipore, USA).

Preparation of the Inclusion Complex of CAH-γCD and **Electrospinning Process.** The CAH-γCD inclusion complex (IC) was prepared by 2:1 molar ratio (guest/CD). Here, γCD (23% w/v) was dissolved in water, and then, CAH was put into the clear aqueous solution of  $\gamma$ CD. It was stirred overnight at room temperature, and the color of the solution turned into white by the formation of inclusion complex crystals. Subsequently, pullulan powder (20%, w/v, with respect to solvent) was added into the CAH-γCD-IC system and stirred till the polymer dissolved completely. The control samples were prepared from pure pullulan, pullulan/ $\gamma$ CD, and pullulan/CAH solutions. Here, pullulan concentration was set as 20% (w/v) for all systems, and the initial CAH content was kept as  $\sim 10.2\%$  (w/w, with respect to total sample amount) for pullulan/CAH and pullulan/ CAH-γCD-IC systems. Electrospinning was conducted using an equipment designed for the process (Spingenix, model: SG100, Palo Alto, USA). Here, electrospinning solutions were separately loaded into disposable syringes, and then, these syringes were located horizontally to the syringe pump. The high voltage (in the range of 15-18 kV) was applied to the stainless-steel needle (23 or 27 G) that was fixed to the syringes. The electrospinning solution was simultaneously pumped by syringe pump with a constant flow rate (0.5 mL/h), and the nanofibrous mat (NM) was deposited on the fixed metal collector wrapped with a piece of Al foil (~25% relative humidity and ~20 °C).

**Structural Characterization.** The fibrous morphology of pullulan NM, pullulan/ $\gamma$ CD NM, pullulan/CAH NM, and pullulan/CAH- $\gamma$ CD-IC NM was examined by scanning electron microscopy (SEM, Tescan-MIRA3). The charging problem of samples was overcome by coating them with a thin layer of Au/Pd prior SEM measurements. The average fiber diameter (AFD, mean  $\pm$  standard deviation) was calculated using ImageJ software (~100 nanofibers). A capillary flow porometer (1100-AEHXL, Porous Media Inc., Ithaca, NY, USA) was used to determine the average pore size (nm) and air permeability (mm/s) of nanofibrous mats. Silwick having a surface

tension of 20.1 dynes/cm was used as the wetting agent during poresize measurement. Here, circular pieces ( $\phi = \sim 26$  mm) from different locations of nanofibrous mats were cut (weight =  $\sim 12-19$  mg and thickness =  $\sim 0.08-0.12$  mm). For air permeability, a maximum differential pressure ( $\Delta P$ ) of  $\sim 300$  Pa was used according to ASTM International (American Society for Testing and Materials) criteria for surgical mask. At least three measurements were conducted for each sample to reach the results as mean values  $\pm$  standard deviations.

An X-ray diffractometer (Bruker D8 Advance ECO) was used to define the X-ray diffraction patterns of  $\gamma$ CD, pullulan NM, pullulan/ γCD NM, pullulan/CAH NM, and pullulan/CAH-γCD-IC NM. XRD scanning was conducted by Cu K $\alpha$  radiation ( $2\theta = 5^{\circ}-30^{\circ}$ , 40 kV, and 25 mA). The attenuated total reflectance Fourier transform infrared spectrometer (ATR-FTIR, PerkinElmer, USA) was used to record the FTIR spectra of CAH,  $\gamma$ CD, pullulan NM, pullulan/ $\gamma$ CD NM, pullulan/CAH NM, and pullulan/CAH-γCD-IC NM (4000-600 cm<sup>-1</sup>, resolution: 4 cm<sup>-1</sup>, 64 scans). A thermogravimetric analyzer (TGA, Q500, TA Instruments, USA) and differential scanning calorimeter (DSC, Q2000, TA Instruments, USA) were used to evaluate the thermal profiles of CAH,  $\gamma$ CD, pullulan NM, pullulan/γCD NM, pullulan/CAH NM, and pullulan/CAH-γCD-IC NM. The TGA and DSC measurements were respectively performed at 30-600 °C with a heating rate of 20 °C/min and at 0-230 °C with a heating rate of 10 °C/min (N<sub>2</sub>).

Loading Efficiency and Time-Dependent Storage Stability Tests. The loading efficiency of nanofibrous mats just after the electrospinning process was examined by dissolving samples in the blend solvent system of ethanol/water (3/7, v/v) (n = 3). The prepared solutions were checked with UV-vis spectroscopy (PerkinElmer, Lambda 35), and the absorption intensity value of graphs at 290 nm was adapted to the calibration curve of CAH in ethanol/water (3/7, v/v) to attain results in terms of % (w/w, with respect to total sample amount). On the other hand, the timedependent storage stability of CAH preserved in the pullulan/CAH NM and pullulan/CAH-γCD-IC NM was followed by proton nuclear magnetic resonance (<sup>1</sup>H-NMR) measurements because this also enabled the simultaneous checking of the chemical structure of CAH under the storage conditions. An NMR spectrometer having an autosampler (NMR, Bruker AV500) was run for the <sup>1</sup>H-NMR measurements. For this, CAH, pullulan/CAH NM and pullulan/ CAH- $\gamma$ CD-IC NM were dissolved in  $d_6$ -DMSO (60 mg/mL), and <sup>1</sup>H-NMR measurements were completed by 16 scans. The <sup>1</sup>H-NMR spectrum of the samples was plotted and processed using the software of Mestranova. For the calculations, the integration of the distinct peaks of components was proportioned, and the results were attained in terms of the molar ratio. To check the prolonged storage stability of nanofibrous mats, they were kept at the conditions of 20-22 °C and 60-65% relative humidity. Afterward, <sup>1</sup>H-NMR measurements were conducted for the samples which were kept at given particular environmental conditions for 1 day, 1 week, and 2 and 4 weeks. The <sup>1</sup>H-NMR results obtained in terms of molar ratio were converted to % (w/w, with respect to total sample amount) to determine the remaining CAH amount in the samples after the given time periods.

**Antibacterial Test.** The antibacterial performance of pullulan/ γCD NM, pullulan/CAH NM and pullulan/CAH-γCD-IC NM was tested against Escherichia coli (E. coli) (BL21 (NEB)) and Staphylococcus aureus (S. aureus) (ATCC 25923) by disk-diffusion assay. These strains were streaked on LB-agar plates and grown overnight at 37 °C. Colonies were diluted in sterile 1× PBS to a McFarland standard of ~0.5. Sterile cotton swabs were then used to spread bacteria onto LB-agar plates. Samples were cut into circular pieces with ~15 mm diameter having identical weight (~13 mg). As a positive control, 20 µL of streptomycin solution (50 mg/mL) was added to filter papers having the same diameter with nanofibers (~15 mm). Three pieces of each sample were placed on an agar plate separately, and plates were incubated in a 37 °C incubator for ~24 h (n = 3). Photos of the bacterial growth on plates were acquired in the Bio-Rad ChemiDoc Image Acquisition system, and zones of inhibition were calculated from these photos.

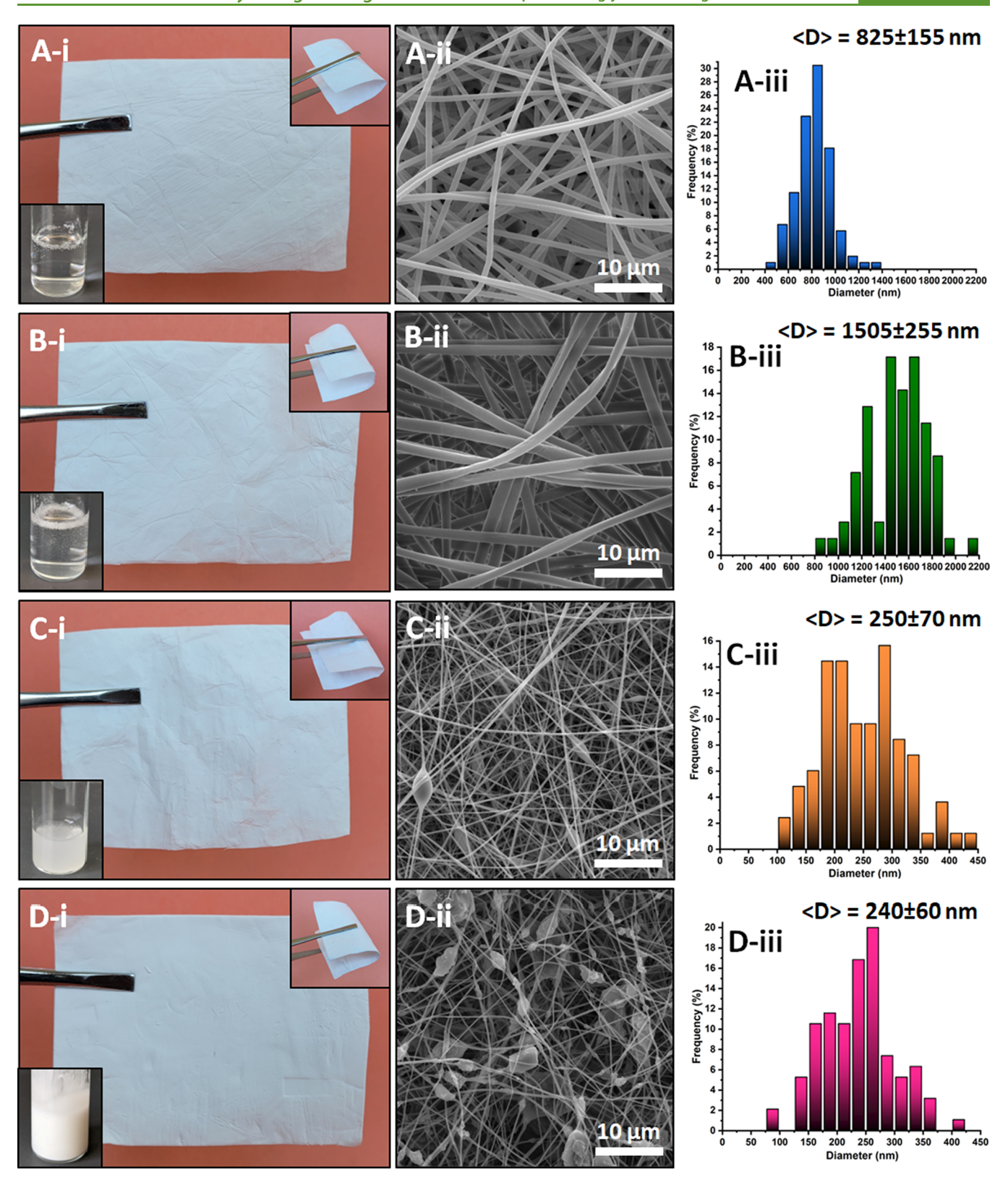


Figure 2. (i) Electrospinning solution/electrospun mat photos, (ii) SEM images, and (iii) diameter distribution of (A) pullulan NM (B) pullulan/γCD NM, (C) pullulan/CAH NM, and (D) pullulan/CAH-γCD-IC NM.

Water Vapor Permeability Measurement, Humidity Stability, and Disposal Tests. Water vapor permeability of the pullulan/ CAH- $\gamma$ CD-IC NM and a surgical face mask having the same thickness ( $\sim$ 0.35 mm) were comparatively examined in accordance with BS 7209:1990 test method.<sup>38</sup> For this, samples were cut into circler pieces having the proper size to seal over the open mouth of the test

dishes that contained water (46 mL). Then, the dishes were located in a control atmosphere (21  $^{\circ}$ C, 65% RH), and their weightings were made at the predetermined time points to determine the rate of water vapor permeation through the samples. The water vapor permeability (WVP; g/m²/day) was calculated by using the equation; WVP = 24M/At, where M is the loss in mass of the test dish at the definite

time point (g); t is the time point of the weighing of the dish (h); and A is the area of the exposed sample (m<sup>2</sup>).

To determine the humidity stability of pullulan/CAH- $\gamma$ CD-IC NM, it was inserted into the pocket of a cloth mask and was kept in a desiccator of which inner conditions were arranged as 99% RH and 37 °C to simulate the extrema environment that can occur when a surgical face mask is worn. <sup>39,40</sup> For this, the bottom of the desiccator was filled with distilled water, and then, the desiccator was located into the oven at 37 °C. The sample was kept in this chamber for 24 h; meanwhile, the RH and temperature were recorded using a digital humidity/temperature reader. On the other hand, the disposal of pullulan/CAH- $\gamma$ CD-IC NM was carried out by washing the sample under tap water, and Video S1 was recorded simultaneously.

**Statistical Analyses.** Statistical analyses were performed using the one-way/two-way of variance followed by Tukey's test (ANOVA). OriginLab (Origin 2021, USA) was used for all these ANOVA analyses (0.05 level of probability).

#### RESULTS AND DISCUSSION

Morphological Features of Nanofibrous Mats. In this study, CAH-γCD inclusion complexes (IC) were incorporated into pullulan nanofibrous mats in one step by dissolving the polymer in the aqueous medium in which the inclusion complexes formed as the suspension and was electrospun into nanofibrous mat (NM). Here, pullulan NM, pullulan/γCD NM, and pullulan/CAH NM were also generated as control samples. Table S1 shows the solution properties of each system used for the electrospinning process and the average fiber diameter (AFD) of electrospun NM. Figure 2i indicates the photos of electrospinning solutions having a clear view for pullulan and pullulan/γCD, while it is turbid and white for pullulan/CAH and pullulan/CAH-γCD-IC due to the emulsion of CAH and suspension of CAH-γCD-IC, respectively. As seen in Figure 2i again, all these systems were achieved into free-standing, flexible, and easily foldable nanofibrous mats. The SEM images of nanofibrous mats revealed the homogenous and bead-free morphology of pullulan and pullulan/γCD systems having AFD values of  $825 \pm 155$  and  $1505 \pm 255$  nm, respectively (Figure 2A,Bii). On the other hand, there were detected few beads within pullulan/CAH NM arising probably from the emulsion nature of the electrospinning solution having oil drop parts of CAH in the electrospinning jet of the relevant system (Figure 2Cii). 41,42 For pullulan/CAH-γCD-IC NM, it was noticed that the inclusion complex crystals were dispersed through the fibrous structure (Figure 2Dii). As seen in Table S1, the addition of yCD increased the viscosity and decreased the conductivity of pullulan solution which resulted in less stretching of electrospinning jet and so thicker fiber formation for pullulan/ $\gamma$ CD NM compared to pristine pullulan NM.<sup>43</sup> In contrast, the addition of CAH and CAH-γCD-IC significantly increased the conductivity of the systems (Table S1). Therefore, AFD of pullulan/CAH NM (250  $\pm$  70 nm) and pullulan/CAH-γCD-IC NM (240 ± 60 nm) was detected significantly lower compared to CAH free-systems. Here, the higher number of charges occurred on the electrospinning jet having high conductivity caused more repulsion and so leaded to higher stretching of jet during the process. On the other hand, the viscosity of the pullulan system did not change apparently with the addition of CAH, while inclusion complex crystal existence caused a more prominent increase in the electrospinning solutions compared to others (Table S1). In other words, complex crystals suspended in the pullulan solution induced a higher resistance against the applied shear

rate during viscosity measurements. However, this did not result in lower stretching over electrospinning and so thicker fiber formation since a monolith response could not be created within the jet during the process due to the heterogeneous distribution of complex crystals around polymer chains.

The average pore size (APS) and air permeability profile of the nanofibrous mats were determined using a capillary flow porometer, and the results are listed in Table S1. The APS of pullulan NM and pullulan/ $\gamma$ CD NM was found to be 456  $\pm$  42 and  $483 \pm 31$  nm, respectively. On the other hand, the APS of pullulan/CAH NM and pullulan/CAH-γCD-IC NM was detected as 203  $\pm$  50 and 391  $\pm$  38 nm, respectively. Even though there was not a clear trend in the relation between pore size and fiber diameter, the APS varied more or less related to the AFD values of nanofibrous mats (Table S1). As expected, bigger pore sizes were observed for the nanofibrous mats which were obtained with thicker fiber diameters. The statistical analysis revealed that the APS value of pullulan/CAH NM  $(203 \pm 50 \text{ nm})$  was significantly different among others (p < 0.05). Here, for the CAH-included sample, it was also obvious that the APS of pullulan/CAH- $\gamma$ CD-IC NM was higher than pullulan/CAH NM even they had a very similar AFD range. This might be attributed inclusion complex crystals which aligned throughout the fiber in the case of pullulan/CAHγCD-IC NM. These crystals might have disturbed the compactivity of fiber arrangements and this might have resulted in the formation of bigger gaps and so bigger pores between fibers. Fortunately, the APS of pullulan/CAH-γCD-IC NM was found to be ~390 nm, which is already smaller than the aerosol size ( $<5 \mu m$ ). This value can be also acceptable and attractive for viral size ranges (20-400 nm) and for the most penetrating particle size ( $\sim$ 0.3  $\mu$ m) defined by the National Institute of Occupational Safety and Health (NIOSH).44,45 On the other hand, the air permeability identifying the rate of airflow that can pass through the surface informs about its breathability, and this is also an essential feature for the potential face mask materials. 9,46 Here, the air permeability values of nanofibrous mats are summarized in Table S1. As expected, there was an approximate correlation between air permeability and the APS of samples, and the air permeability value of pullulan/CAH NM was found to be significantly different compared to others (p < 0.05). For pullulan/CAH-γCD-IC NM, the air permeability was detected as  $32.6 \pm 2.1$  mm/s, and this result was in accordance with, even better than, the previous studies in which the air permeability values were reported in the range of 10–20 mm/s for the electrospun nanofibers of different polymers including polyethylene terephthalate (PET),<sup>47</sup> cellulose acetate (CA),<sup>48</sup> and polyurethane (PU).<sup>49</sup> As reported by Ullah et al., the air permeability feature of electrospun nanofibers (~17.0 cfm) is still not as good as the melt-blown fiber ( $\sim$ 27.2 cfm) already used for the commercial face masks. This is because of the nano-sized porosity of electrospun fibers that contrarily provides an advantage from the point of filtration performance.<sup>50</sup> On the other hand, there has been an notable effort in the literature to improve the comfort properties of electrospun nanofibers. 46-52 Even one of the optimization studies reporting the effect of electrospun mat thickness on the air permeability feature indicated that this feature can be easily manipulated by changing the thickness of collected the nanofibrous mats.<sup>5</sup>

**Structural Character of Nanofibrous Mats.** X-ray diffractometry (XRD) profile of samples was analyzed to confirm the inclusion complex existence within the nanofibrous

mats (Figure S1). Figure S1B displays the XRD pattern of pristine  $\gamma$ CD powder, pullulan NM, pullulan/ $\gamma$ CD NM, pullulan/CAH NM, and pullulan/CAH-γCD-IC NM. Pristine γCD is known to have a "cage-like" crystalline packing where CD cavities are being blocked by the neighboring ones as described schematically in Figure S1A. This type of crystalline packing creates XRD pattern having peaks at  $2\theta = 5.2^{\circ}$ ,  $12.4^{\circ}$ , 14.0°, 16.5°, 18.8°, and 21.8° (Figure S1B). However, in case of a successful complexation, \( \gamma CD \) molecules reorganize into the "channel-type" lattice as the  $\gamma$ CDs stack on top of each other to form cylindrical channels, showing distinct peaks at  $2\theta$ =7.0°, 14.0°, 15.0°, 16.0°, and 17.0° (Figure S1A, B). 53 Here, pristine pullulan NM showed a broad peak positioned at  $2\theta$  = 18.5° that is due to the *d*-spacing of 4.52 Å. 54 As expected, pullulan/CAH NM which is a physical mixture of pullulan and essential oil molecules depicted the similar diffraction profile with pristine pullulan NM (Figure S1B). This is unlike the XRD pattern of pullulan/CAH-γCD-IC NM where the amorphous profile of pullulan was dominated by the characteristic peaks of the CAH-γCD-IC crystalline structures (Figure S1B). Here, the intense peaks at the XRD spectrum of pullulan/CAH-γCD-IC NM belong to the "channel-type" of packaging as described above and evidence of the distribution of the inclusion complex crystals within this nanofibrous mat.<sup>27,53</sup> XRD results further validated the SEM imaging findings in which the crystals of CAH-γCD-IC were clearly visible in the fibrous matrix (Figure 2Dii).

The structural analysis of CAH,  $\gamma$ CD, and nanofibrous mats of pullulan, pullulan/γCD, pullulan/CAH, and pullulan/CAHγCD-IC was further characterized using Fourier transform infrared (FTIR) spectroscopy (Figure S2). In the FTIR spectrum of CAH, significant peaks were detected at 1670 and 1624 cm<sup>-1</sup> corresponding to stretching of  $\nu$ (C=O) and conjugated alkene  $\nu(C=C)$ . The skeleton vibrations of the benzene ring appeared at 1575, 1495, 1450, 1120, 745, and 687 cm<sup>-1</sup>. There were also significant peaks at 1294 and 971 cm<sup>-1</sup> due to the  $\nu$ (C-H) in-plane bending of -CHO and deformation of conjugated alkene  $\nu(C=C)$ , respectively. 55,56 In the case of  $\gamma$ CD, the spectrum showed stretching bands at 3266 cm<sup>-1</sup> for symmetrical and asymmetrical stretching of  $\nu$ (O-H). The stretching of methyl/methylene  $\nu$ (C-H) was observed at 2925 cm<sup>-1</sup>. The H-O-H bending, asymmetric  $\nu(C-O-C)$  link stretching, and the  $\nu(C-O)/\nu(C-C)$ stretching were also detected at 1641, 1153, and 1077 cm<sup>-1</sup>/ 1020 cm<sup>-1</sup>, respectively.<sup>27</sup> It was found that the characteristic bands of  $\gamma CD$  were quite similar to those observed from pristine pullulan NM, which exhibited absorption peaks located at 3313, 2925, and 1641 cm<sup>-1</sup>, that attributed to the  $\nu({\rm O-H})$  stretching,  $\nu({\rm C-H})$  stretching, and H–O–H bending, respectively.  $^{\rm S7,58}$  The overlap between the spectra of these two components can be explained by the similarities between their molecular structures.  $\gamma$ CD is constructed of  $\alpha$ -(1,4) linked glucopyranose sub-units (Figure 1A), which are similar to the maltotriose (three glucose units linked by  $\alpha$ -(1,4) glycosidic bonds) units that connected themselves by  $\alpha$ -(1,6) glycosidic bonds and make up the pullulan polymer (Figure 1A).<sup>57</sup> This similarity resulted in analogous absorption bands at the parallel region of the spectrum for  $\gamma$ CD and pullulan (Figure S2). Here, the FTIR spectrum of pullulan/ CAH-γCD-IC NM was compared with pullulan/γCD NM to clearly follow the difference arising from the CAH content (Figure S2Bi). For pullulan/CAH-γCD-IC NM, the characteristic peaks of CAH highlighted in the expanded spectra with

vertical lines and asterisk (\*) confirmed the presence of this essential oil compound in the nanofibrous mat. Moreover, there were detected shifts for the characteristic peaks of CAH at 1670, 1624, 1294, 1120, 971, and 687 cm<sup>-1</sup> to 1678, 1625, 1297, 1105, 937, and 684 cm<sup>-1</sup>, respectively, in case of pullulan/CAH-γCD-IC NM (Figure S2Bi). This alteration also verified the inclusion complex formation between CAH and γCD encapsulated in electrospun nanofibrous mat. On the other hand, the given peaks of CAH were not mostly observed in the FTIR spectrum of pullulan/CAH NM; just the most distinct peaks of CAH at 1670 and 1624 cm<sup>-1</sup> enhanced the intensity at the same region of pullulan/CAH NM compared to pullulan NM (Figure S2Bii). This finding might be explained by the higher amount of CAH preserved and so encapsulated in pullulan/CAH-γCD-IC NM compared to pullulan/CAH NM due to inclusion complexation. This result was further demonstrated by the other characterization techniques explained in the next sections.

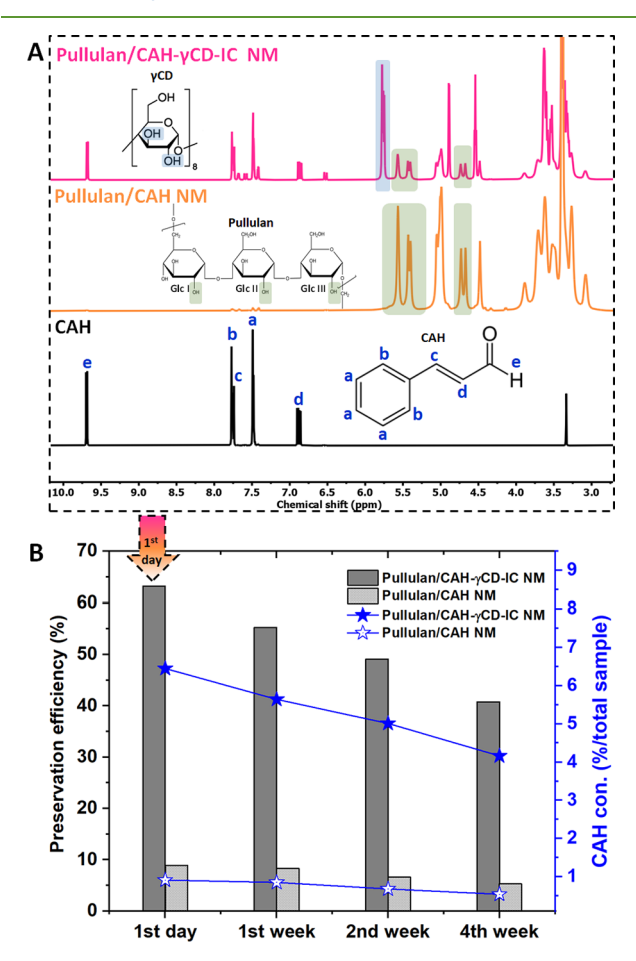
The thermal decomposition profiles of samples were examined using thermogravimetric analysis (TGA). The thermograms and the derivatives (DTG) of CAH, pullulan NM, pullulan/CAH NM, pullulan/γCD NM, and pullulan/ CAH-γCD-IC NM are given in Figure S3. The volatile nature of CAH was validated by TGA measurement, in which the evaporation of CAH started at ~40 °C and completed at ~185 °C (Figure S3). The thermograms of pullulan NM and pullulan/γCD NM can be described by two main weight losses: (i) the dehydration of water till ~100-120 °C and (ii) the main degradation of the sample at  $\sim$ 325-330 °C. The thermogram of the pullulan/CAH NM showed similarity with that of the pristine pullulan NM, where two weight losses were detected corresponding to the dehydration of water (till ~130 °C) and the main degradation of pullulan (~325 °C) (Figure S3B). Here, the physically mixed CAH within pullulan NM was not observed in the thermogram or in its DTG as a split weight loss (Figure S3B). This result can be explained by CAH volatilization that occurred in a similar temperature range as the dehydration of water and also by the loss of a huge amount of CAH that could not be protected during the process. On the other hand, the thermogram of pullulan/CAH-\(gamma\)CD-IC NM displayed an additional small weight loss step apart from water dehydration (~120 °C) and main degradation (330 °C) steps (Figure S3A). This additional weight loss took place at  $\sim$ 273 °C and corresponded to the volatilization of CAH that is encapsulated in the  $\gamma$ CD cavity by inclusion complexation (Figure S3Aii). Principally, the complexation with CD can result in a shift of the thermal degradation or volatilization of guest molecules to a higher temperature. 59,60 It is clear that there is a shift from  $\sim 171$  to  $\sim 273$  °C for the thermal volatilization of CAH in the case of pullulan/CAH-γCD-IC NM compared to pure CAH. Here, the interaction with the cavity of  $\gamma$ CD leaded to a volatilization process that required higher range of temperatures to occur and thus revealed the increased thermal stability of CAH through inclusion complexation.

Figure S4 shows differential scanning calorimetry (DSC) thermograms of CAH, pullulan NM, pullulan/ $\gamma$ CD NM, pullulan/CAH NM, and pullulan/CAH- $\gamma$ CD-IC NM. Here, there was no specific endothermic peak detected for pure CAH due to its liquid nature in the given temperature range. On the other hand, DSC thermograms of pullulan NM and pullulan/ $\gamma$ CD NM, respectively, displayed endothermic peaks at ~82 and ~88 °C based on the dehydration of water (Figure

S4).  $^{61,62}$  It is clear that the incorporation of  $\gamma$ CD in pullulan NM leaded to a shift at the dehydration temperature to a higher temperature. Additionally, the peak area representing the  $\Delta H$  value and corresponding to the energy required for the thermal transition increased from 263 to 350 J/g with the addition of  $\gamma$ CD (Figure S4A). These results can be explained by the increased crystal water content in the sample arising from the  $\gamma$ CD structure and so the need for a higher amount of energy to remove it from the substrate. Essentially, the incorporation of an additional compound into nanofibrous mats might stimulate a shift in the thermal transition temperature of the carrier polymeric matrix.<sup>63</sup> In our study, the dehydration temperature of pullulan/γCD NM (~88 °C) shifted to lower temperature (~81 °C) in case of pullulan/ CAH-γCD-IC NM. Moreover, the endothermic peak of dehydration became sharper in shape and decreased in terms of the  $\Delta H$  value from 350 to 236 J/g (Figure S4A). This result also supported the incorporation of pullulan NM with the inclusion complex crystals in which \( \gamma CD \) cavities were occupied with the essential oil compounds of CAH instead of crystal water molecules differently from the pristine  $\gamma$ CD cavities. Therefore, less amount of energy was needed to evaporate the water molecules within the structure for pullulan/CAH-γCD-IC NM when compared to pullulan/ γCD NM. In the case of pullulan/CAH NM, the thermal transition profile took part by having almost the same profile as pullulan NM due to the physical blending of pullulan and CAH and the tiny amount of CAH that could be preserved in pullulan/CAH NM (Figure S4B).

Long-Term Storage Stability Results. As it has been reported in our related studies,  $\gamma$ CD enabled the preparation of electrospinning solutions and so the ultimate nanofibrous mats with the high inclusion complex content due to its higher solubility (23%, w/v) in water compared to  $\beta$ CD (1.85%, w/ v). 27,64 Thus, high concentrations of essential oils can be incorporated into electrospun nanofibrous mats (~10%, w/w, with respect to total sample amount). In other related studies, it was depicted that CAH can form inclusion complexes with  $\beta$ CD having the 1:1 molar ratio (CAH/CD). 65,66 On the other hand, the molecular modeling analysis previously reported by Yildiz et al. revealed that the hydroxypropylated derivative of  $\gamma$ -CD (HPγCD) can form more effective inclusion complexes in the aqueous medium compared to HP $\beta$ CD in the case of 2:1 molar ratio (CAH/CD).<sup>34</sup> Here, HPγCD showed energetically more favorable complexation profile than HP $\beta$ CD due to better size match between CAH and HPγCD.<sup>34</sup> Due to these reasons, we prepared the electrospinning solutions using  $\gamma$ CD and having a 2:1 (CAH/CD) molar ratio that corresponded to the 10.2% (w/w) CAH content. It is noteworthy to mention that this high loading quantity did not cause any trouble during the electrospinning process of both CAH- and CAH-γCD-ICcontaining systems. The loaded CAH within the nanofibrous mats thereafter electrospinning process was examined by dissolving samples in the ethanol/water (3/7, v/v) blend system. The results showed that pullulan/CAH NM and pullulan/CAH-γCD-IC NM were produced having a loading efficiency of 9.9  $\pm$  0.8 and 61.9  $\pm$  0.7%, corresponding to the CAH concentrations of 1.0  $\pm$  0.1 (w/w) and 6.3  $\pm$  0.1% (w/ w), respectively. It is obvious that a meaningfully higher amount of CAH was preserved for pullulan/CAH-\(\gamma\)CD-IC NM compared to pullulan/CAH NM owing to encapsulation of CAH into cyclodextrin voids by inclusion complexation. In the case of pullulan/CAH NM, CAH molecules were in an uncomplexed state, so this highly volatile compound was lost by the evaporation from the pullulan matrix during the electrospinning process. The significant difference between the loading efficiencies of samples was also statistically confirmed with p < 0.05 value.

In this study, the <sup>1</sup>H-NMR technique was applied to detect the CAH content of nanofibrous mats kept at room temperature for the prolonged storage stability test and also for analyzing the chemical structure of CAH under the storage conditions. Figure 3A displays the representative <sup>1</sup>H-NMR



**Figure 3.** (A)  $^{1}$ H-NMR spectra of CAH, pullulan/CAH NM, and pullulan/CAH- $\gamma$ CD-IC NM. (B) Time-dependent stability graph of CAH loaded (%) in pullulan/CAH NM and pullulan/CAH- $\gamma$ CD-IC NM

spectra of CAH, pullulan/CAH- $\gamma$ CD-IC NM, and pullulan/CAH NM that were recorded the following day of the electrospinning process (1st day). Here, the discrete peaks of CAH,  $\gamma$ CD, and pullulan positioned at 6.8–9.8, 5.8, and 5.3–5.6 ppm, respectively, were chosen for the calculations (Figure 3A). The CAH content was found to be ~6.5 (w/w) and ~0.9% (w/w) for pullulan/CAH- $\gamma$ CD-IC NM and pullulan/CAH NM, which showed that ~63.2 and ~8.9% of the initial CAH content (~10.2% (w/w)) was preserved for the given samples, respectively. The findings of the 1st day are approximately correlated with the previous calculations which were performed thereafter the electrospinning process and where the loading efficiency of pullulan/CAH- $\gamma$ CD-IC NM and pullulan/CAH NM was respectively detected as 61.9  $\pm$  0.7 and 9.9  $\pm$  0.8%. Figure 3B further indicates preservation

efficiency (%) and the CAH content (%, w/w) values of nanofibrous mats recorded for 1-week, 2-week, and 4-week storage periods. At the end of four weeks, it was observed that the CAH content was calculated as  $\sim$ 4.2 (w/w) and  $\sim$ 0.5% (w/w) for pullulan/CAH-γCD-IC NM and pullulan/CAH NM, respectively. This displayed that ~40.8 and ~5.3% of the initial CAH content remained in the nanofibrous mats of pullulan/CAH-γCD-IC and pullulan/CAH, respectively, over this time period. In other words, pullulan/CAH-γCD-IC NM ensured approximately eight times higher CAH content compared to pullulan/CAH NM after this prolonged storage. These findings demonstrated that the inclusion complexation provided an efficient loading efficiency for CAH during the electrospinning process, and a significantly better long-term storage stability for this essential oil molecule encapsulated in nanofibrous mats. The conserved chemical structure of CAH during the storage period was also confirmed through <sup>1</sup>H-NMR findings in which the characteristic peaks of this active compound in nanofibrous mats were observed in the same way as pure CAH molecules (Figure S5). As expected, the characteristic peaks of CAH were observed with a higher intensity in the case of pullulan/CAH-\gammaCD-IC NM (Figure SSB) compared to pullulan/CAH NM (Figure SSC) that accommodate to the higher CAH content of pullulan/CAHγCD-IC NM, and this trend was followed along a storage period over 4 weeks.

Antibacterial Performance of Nanofibrous Mats. The antibacterial potential of pullulan/CAH NM and pullulan/CAH-γCD-IC NM was examined against gram positive (*S. aureus*) and gram negative (*E. coli*) bacteria using disk-diffusion method. The photos of the test plates are given in Figure 4,

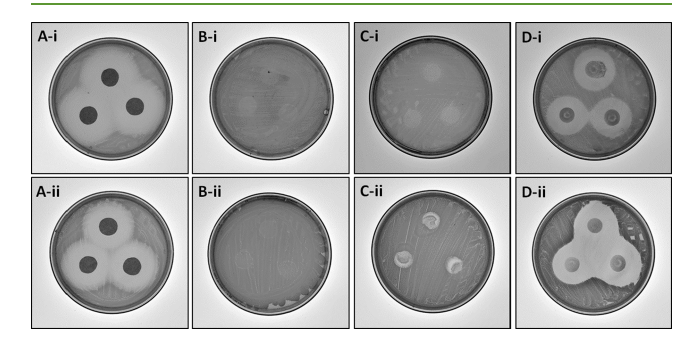


**Figure 4.** Photos of antibacterial test of (A) filter paper impregnated with Streptomycin solution, (B) pullulan/ $\gamma$ CD NM, (C) pullulan/CAH NM, and (D) pullulan/CAH- $\gamma$ CD-IC NM against (i) *E. coli* and (ii) *S. aureus* strains.

and the diameters of inhibition zones determined from these photos are listed in Table 1. The positive control; filter paper impregnated with the solution of broad-spectrum antibiotic drug (streptomycin), and having the same diameter as nanofibrous mats ( $\sim$ 15 mm) displayed transparent circles

Table 1. Diameter (mm) of Bacterial Inhibition Zones of Samples $^a$ 

bacteria strain	filter paper/ streptomycin	pullulan/ γCD NM	pullulan/ CAH NM	pullulan/CAH- γCD-IC NM
E. coli	$49.3 \pm 1.3$			$32.8 \pm 1.4$
S. aureus	$43.6 \pm 2.5$			$35.9 \pm 1.4$

<sup>&</sup>lt;sup>a</sup>Sample diameter: ∼15 mm.

due to inhibition of bacterial growth (Figure 4Ai,ii). The statistical analysis confirmed the difference between the antibacterial activity of the control sample against E. coli and S. aureus to be significant with an inhibition zone diameter of  $49.3 \pm 1.3$  and  $43.6 \pm 2.5$  mm, respectively (p < 0.05) (Table 1). Being a broad-spectrum antibiotic, streptomycin shows principally similar antibacterial activity against both grampositive and gram-negative bacteria such as S. aureus and E. coli; the observed relative variations in the inhibition performance may be assigned to gradual permeation behavior from the cell membranes or relative uptake from receptors of different organisms.  $^{67}$ 

Antibacterial activity was not detected for the control sample of pullulan/γCD NM (Figure 4Bi,ii). For the other control sample of pullulan/CAH NM, an inhibition activity was detected just within the border of the sample with tiny spots having an uneven shape and without a distinct inhibition zone formation against both E. coli and S. aureus (Figure 4C-i,ii). On the other hand, pullulan/CAH-γCD-IC NM displayed an antibacterial effect with the inhibition zone diameter of 32.8  $\pm$ 1.4 and 35.9  $\pm$  1.4 mm for E. coli and S. aureus, respectively (Table 1 and Figure 4Di, ii). The statistically significant difference between the inhibition zones for E. coli and S. aureus for pullulan/CAH- $\gamma$ CD-IC NM was proved with the p = 0.049value. Similar finding was also reported by Yang et al., and the slightly better inhibition property against S. aureus compared to E. coli was assigned to a phenomenon which explains that the penetration of hydrophobic CAH was partially reduced by the hydrophilic outer membrane of E. coli (Gram negative bacteria).<sup>68</sup> It is obvious that pullulan/CAH-γCD-IC NM showed an apparent antibacterial activity similar to the positive control streptomycin. Here, the superior antibacterial performance of pullulan/CAH-γCD-IC NM shown with a clear inhibition zone formation compared to pullulan/CAH NM (Figure 4 and Table 1) was due to its higher loading efficiency (~62%) provided by inclusion complexation than pullulan/ CAH NM ( $\sim$ 10%). This resulted in higher and better participation during the bacterial inhibition over a higher amount of CAH. Moreover, the potential enhancement that can be observed for the water solubility of the hydrophobic CAH molecule by inclusion complexation<sup>32,34</sup> might have contributed to the easier penetration of CAH in the agar medium, and this might have supported its antibacterial property.

Water Vapor Permeability, Humidity Stability, and **Disposal Profiles.** As discussed in the previous sections, pullulan/CAH-γCD-IC NM indicated better CAH preservation and antibacterial performance along with more acceptable pore size and air permeability features compared to pullulan/ CAH NM. Therefore, the water vapor permeability (WVP) test was carried out for pullulan/CAH-\gammaCD-IC NM by comparison with a standard surgical face mask (Figure S6). Figure S6 indicates the weight loss recorded for the samples as a function of time with a good linear fitting  $(R^2 = 1)$ . WVP is a crucial feature for the breathability and comfort profile of face mask materials. Here, the WVP was found to be ~890 and  $\sim 1025 \text{ g/m}^2/\text{day for pullulan/CAH-}\gamma \text{CD-IC NM and surgical}$ face mask, respectively. As seen, nanofibrous mat showed a lower WVP value compared to the commercial face mask for the same sample thickness of ~0.35 mm. This might be the consequence of the nanofibrous-based sample's nano-scaled properties, which might have relatively inhibited vapor molecule transmission when it is compared to the surgical

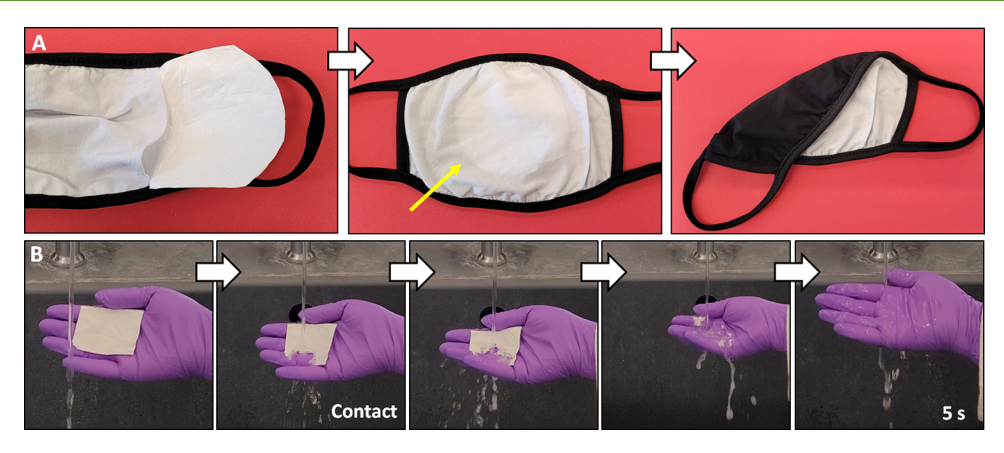


Figure 5. (A) Insertion photos of pullulan/CAH-γCD-IC NM into the pocket of a fabric face mask. (B) Dissolving of pullulan/CAH-γCD-IC NM by washing under tap water (photos were captured from Video S1).

face mask. However, it is possible to alter the WVP value of pullulan/CAH- $\gamma$ CD-IC NM by modifying its thickness because as it has been reported in the previous studies that higher WVP values can be detected in the range of 1300–1400 g/m²/day for the electrospun nanofibrous samples having a thickness at around 0.17–0.18 mm.  $^{47,69}$  In addition to this, it is not required to produce pullulan/CAH- $\gamma$ CD-IC NM with the same thickness as an ultimate surgical face mask. Because pullulan/CAH- $\gamma$ CD-IC NM was developed as a potential functional layer that can be easily inserted into a fabric-based face mask's pocket owing to the self-standing, flexible, and foldable features of the nanofibrous mats (Figure 5A).

Since the pullulan and  $\gamma$ CD has hydrophilic nature, the stability of pullulan/CAH-\u03c4CD-IC NM was also examined under the extrema conditions (99% RH and 37 °C) of humid environment that might occur when worn a surgical face mask. For this, pullulan/CAH-γCD-IC NM was inserted in the pocket of a surgical face mask and kept at these conditions for 24 h (Figure S7A). It was detected that the area of the nanofibrous mat decreased by ~4 times by keeping its shape integrity at the end of the given time period (Figure S7B). However, besides the long term used for this test (24 h), the examined conditions represent the saturated humidity (99% RH) and peak temperature (37 °C) that might be reached at the jumping-off point of the surgical face mask usage.<sup>39,40</sup> Therefore, the detected difference can be considered as the maximum dimensional variation for the developed nanofibrous mat under these given conditions. On the other hand, the hydrophilic nature of pullulan/CAH-γCD-IC NM can be considered as an advantage because one of the main problems of surgical face mask is the layers that are produced from water-resistant polymers such as polypropylene (PP), polystyrene (PS), and so forth. Here, the moisture cannot be wicked away in time, forming condensed water around the micro-environment of the mouth in the mask, and this causes breath resistance and discomfort on face.<sup>70</sup> In contrast, pullulan/CAH-γCD-IC NM can inhibit the formation of condensed water during its usage by holding the exhaled moisture in the progress of time.

In this study, pullulan/CAH- $\gamma$ CD-IC NM was developed as a functional face mask layer that can be alternative to the commercially available face mask products manufactured using synthetic polymers. As known, plastics are identified as one of the main sources of pollution because of their low degradation profile in the environment. On the contrary, pullulan/CAH-

 $\gamma$ CD-IC NM can be easily cleared away thereafter its usage by simply washing using water due to the aqueous solubility property of pullulan and  $\gamma$ CD. Accordingly, Figure 5B and Video S1 show that pullulan/CAH- $\gamma$ CD-IC NM was completely dissolved in 5 s without resulting in a potential loading to the environment owing to the biocompatibility advantage of each component (pullulan,  $\gamma$ CD, and CAH). In other words, pullulan/CAH- $\gamma$ CD-IC NM can provide an easier and faster disposal compared to the commercially available surgical face masks.

#### CONCLUSIONS

To conclude, the electrospinning technique enabled the generation of free-standing, light-weight, and foldable nanofibrous mats (NM) from a biocompatible pullulan polymer by the incorporation of the  $\gamma$ -cyclodextrin ( $\gamma$ CD) inclusion complexes (IC) of a well-known essential oil compound trans-cinnamaldehyde (CAH). Here, pullulan/CAH-γCD-IC NM was developed as a functional layer for inserting into cloth-based face masks by using and adapting "green" and sustainable components and process. Pullulan/CAH-γCD-IC NM was produced in one step by using water, and it was obtained with ~240 nm of average fiber diameter. This fiber size and the inclusion-complex crystals distributing through the fiber matrix provided an average pore size of ~390 nm which would be effective to trap aerosols ( $<5 \mu m$ ) and viral particles (20-400 nm). The enhanced thermal stability of CAH due to inclusion complexation was demonstrated by the shift of volatilization from ~171 to ~273 °C for CAH in the case of pullulan/CAH-γCD-IC NM. Here, the use of CD inclusion complexes ensured significantly higher preservation effect for the volatile CAH molecule, and so pullulan/CAH-γCD-IC NM was fabricated with a loading efficiency of  $\sim$ 62%, while this value was ~10% for the control sample of pullulan/CAH NM. This preservation performance was also observed during prolonged storage and pullulan/CAH-γCD-IC NM and pullulan/CAH NM kept ~41 and ~5% of initial CAH after 4 weeks, respectively. The better preservation yield displayed its outcome on the antibacterial feature and pullulan/CAHγCD-IC NM showed a prominent antibacterial activity against both gram positive (S. aureus) and gram negative (E. coli) bacteria compared to pullulan/CAH NM. The antibacterial activity of pullulan/CAH-γCD-IC NM was a sign of the hygienic micro-environment that would be provided during its application and also the favorable conditions after use for the

further disposal process. In this study, it was also shown that pullulan/CAH-\(\gamma\)CD-IC NM shows a promising and improvable water vapor permeability (~890 g/m²/day) and air permeability (~33 mm/s) properties. Here, the hydrophilic and water-soluble nature of pullulan/CAH-γCD-IC NM can be considered an advantage for both wear comfort and disposal management. Accordingly, it was shown that pullulan/CAH- $\gamma$ CD-IC NM can be disposed of by simply washing under tap water after their usage without a potential environmental burden. Briefly, there is still huge demand and effort for developing face coverings that can eliminate environmental concerns and address comfort issues. In this respect, the use of electrospun nanofibrous mat generated from the renewable pullulan polymer by the incorporation of antibacterial CAH-CD inclusion complexes as a functional layer for the cloth masks can be a rather promising approach. These findings can be another stepping stone for the development of affordable, comfortable, and sustainable face coverings of which importance will not definitely go out of our life in the near future.

#### ASSOCIATED CONTENT

# Supporting Information

The Supporting Information is available free of charge at https://pubs.acs.org/doi/10.1021/acssuschemeng.3c02598.

Structural characterization data of samples (XRD, FTIR, TGA, and DSC); schematic representations and photos for water vapor permeability (WVP); humidity stability tests; and weight loss graphs for WVP test (PDF)

## AUTHOR INFORMATION

# **Corresponding Author**

Tamer Uyar — Fiber Science Program, Department of Human Centered Design College of Human Ecology, Cornell University, Ithaca, New York 14853, United States; orcid.org/0000-0002-3989-4481; Email: tu46@cornell.edu

#### **Authors**

Asli Celebioglu — Fiber Science Program, Department of Human Centered Design College of Human Ecology, Cornell University, Ithaca, New York 14853, United States;

orcid.org/0000-0002-5563-5746

Christopher W. Lawson – Operations Research and Information Engineering, College of Engineering, Cornell University, Ithaca, New York 14853, United States

Emmy Zhiren Hsiung — Fiber Science Program, Department of Human Centered Design College of Human Ecology, Cornell University, Ithaca, New York 14853, United States

Rimi Chowdhury — Department of Population Medicine and Diagnostic Sciences, College of Veterinary Medicine, Cornell University, Ithaca, New York 14850, United States;

ocid.org/0000-0002-4530-0029

Craig Altier – Department of Population Medicine and Diagnostic Sciences, College of Veterinary Medicine, Cornell University, Ithaca, New York 14850, United States

Complete contact information is available at: https://pubs.acs.org/10.1021/acssuschemeng.3c02598

#### **Author Contributions**

A.C. performed conceptualization, methodology, investigation, and writing of the original draft. C.W.L. and E.Z.H. performed

investigation. R.C. performed investigation of antibacterial test and editing. C.A. participated in supervision and resources for antibacterial part. T.U. supervised the study and participated in funding acquisition, project administration, conceptualization, formal analysis, methodology, and review and editing.

#### Notes

The authors declare no competing financial interest.

#### ACKNOWLEDGMENTS

This work made use of the Department of Human Centered Design facilities, Cornell Center for Materials Research (CCMR), supported by NSF MRSEC (DMR-1719875), Cornell Chemistry NMR Facility supported in part by the NSF MRI program (CHE-1531632).

#### REFERENCES

- (1) World Health Organization. Covid-19 global situation (April 2023) https://covid19.who.int/.
- (2) Eikenberry, S. E.; Mancuso, M.; Iboi, E.; Phan, T.; Eikenberry, K.; Kuang, Y.; Kostelich, E.; Gumel, A. B. To Mask or Not to Mask: Modeling the Potential for Face Mask Use by the General Public to Curtail the COVID-19 Pandemic. *Infect. Dis. Model.* **2020**, *5*, 293–308
- (3) Leung, N. H. L.; Chu, D. K. W.; Shiu, E. Y. C.; Chan, K.-H.; McDevitt, J. J.; Hau, B. J. P.; Yen, H.-L.; Li, Y.; Ip, D. K. M.; Peiris, J. S.; Seto, W. H.; Leung, G. M.; Milton, D. K.; Cowling, B. J. Respiratory Virus Shedding in Exhaled Breath and Efficacy of Face Masks. *Nat. Med.* **2020**, *26*, *676*–*680*.
- (4) Sullivan, G. L.; Delgado-Gallardo, J.; Watson, T. M.; Sarp, S. An Investigation into the Leaching of Micro and Nano Particles and Chemical Pollutants from Disposable Face Masks-Linked to the COVID-19 Pandemic. *Water Res.* **2021**, *196*, No. 117033.
- (5) Feng, S.; Shen, C.; Xia, N.; Song, W.; Fan, M.; Cowling, B. J. Rational Use of Face Masks in the COVID-19 Pandemic. *Lancet Respir. Med.* **2020**, *8*, 434–436.
- (6) Liu, W.; Sun, Y.; Cui, A.; Xia, Y.; Yan, Q.; Song, Y.; Wang, L.; Shan, G.; Wang, X. Electrothermal Sterilization and Self-Powered Real-Time Respiratory Monitoring of Reusable Mask Based on Ag Micro-Mesh Films. *Nano Energy* **2023**, *105*, No. 107987.
- (7) Imani, S. M.; Ladouceur, L.; Marshall, T.; Maclachlan, R.; Soleymani, L.; Didar, T. F. Antimicrobial Nanomaterials and Coatings: Current Mechanisms and Future Perspectives to Control the Spread of Viruses Including SARS-CoV-2. ACS Nano 2020, 14, 12341–12369.
- (8) Idowu, G. A.; Olalemi, A. O.; Aiyesanmi, A. F. Environmental Impacts of Covid-19 Pandemic: Release of Microplastics, Organic Contaminants and Trace Metals from Face Masks under Ambient Environmental Conditions. *Environ. Res.* **2023**, *217*, No. 114956.
- (9) Kwong, L. H.; Wilson, R.; Kumar, S.; Crider, Y. S.; Reyes Sanchez, Y.; Rempel, D.; Pillarisetti, A. Review of the Breathability and Filtration Efficiency of Common Household Materials for Face Masks. *ACS Nano* **2021**, *15*, 5904–5924.
- (10) Konda, A.; Prakash, A.; Moss, G. A.; Schmoldt, M.; Grant, G. D.; Guha, S. Aerosol Filtration Efficiency of Common Fabrics Used in Respiratory Cloth Masks. *ACS Nano* **2020**, *14*, 6339–6347.
- (11) Radney, J. G.; Weaver, J. L.; Vicenzi, E. P.; Staymates, M. E.; Zangmeister, C. D. Filter Inserts Impact Cloth Mask Performance against Nano-to Micro-Sized Particles. *ACS Nano* **2021**, *15*, 12860–12868.
- (12) Tuñón-Molina, A.; Takayama, K.; Redwan, E. M.; Uversky, V. N.; Andrés, J.; Serrano-Aroca, Á. Protective Face Masks: Current Status and Future Trends. ACS Appl. Mater. Interfaces 2021, 13, 56725–56751.
- (13) Singh, S. S.; Zaitoon, A.; Arvaj, L.; Balamurugan, S.; Manickavasagan, A.; Lim, L.-T. Biobased Antiviral Nonwoven Mask Filter with High Filtration Performance. *ACS Appl. Eng. Mater.* **2023**, *1*, 646–659.

- (14) Cho, Y.; Son, Y.; Ahn, J.; Lim, H.; Ahn, S.; Lee, J.; Bae, P. K.; Kim, I.-D. Multifunctional Filter Membranes Based on Self-Assembled Core—Shell Biodegradable Nanofibers for Persistent Electrostatic Filtration through the Triboelectric Effect. *ACS Nano* **2022**, *16*, 19451–19463.
- (15) Hazarika, D.; Kalita, N. K.; Kumar, A.; Katiyar, V. Functionalized Poly (Lactic Acid) Based Nano-Fabric for Anti-Viral Applications. *RSC Adv.* **2021**, *11*, 32884–32897.
- (16) Wang, L.; Gao, Y.; Xiong, J.; Shao, W.; Cui, C.; Sun, N.; Zhang, Y.; Chang, S.; Han, P.; Liu, F.; He, J. Biodegradable and High-Performance Multiscale Structured Nanofiber Membrane as Mask Filter Media via Poly (Lactic Acid) Electrospinning. *J. Colloid Interface Sci.* 2022, 606, 961–970.
- (17) Wu, H.; Geng, Q.; Li, Y.; Song, Y.; Chu, J.; Zhou, R.; Ning, X.; Dong, S.; Yuan, D. CuMOF-Decorated Biodegradable Nanofibrous Membrane: Facile Fabrication, High-Efficiency Filtration/Separation and Effective Antibacterial Property. J. Ind. Eng. Chem. 2022, 114, 475–482.
- (18) Lo, J. S. C.; Daoud, W.; Tso, C. Y.; Lee, H. H.; Firdous, I.; Deka, B. J.; Lin, C. S. K. Optimization of Polylactic Acid-Based Medical Textiles via Electrospinning for Healthcare Apparel and Personal Protective Equipment. *Sustain. Chem. Pharm.* **2022**, 30, No. 100891.
- (19) Tian, G.; Huang, Z.; Wang, H.; Cui, C.; Zhang, Y. Polycaprolactone Nanofiber Membrane Modified with Halloysite and ZnO for Anti-Bacterial and Air Filtration. *Appl. Clay Sci.* **2022**, 223, No. 106512.
- (20) Soo, X. Y. D.; Wang, S.; Yeo, C. C. J.; Li, J.; Ni, X. P.; Jiang, L.; Xue, K.; Li, Z.; Fei, X.; Zhu, Q.; Loh, X. J. Polylactic Acid Face Masks: Are These the Sustainable Solutions in Times of COVID-19 Pandemic? *Sci. Total Environ.* **2022**, *807*, No. 151084.
- (21) Chowdhury, M. A.; Shuvho, M. B. A.; Shahid, M. A.; Haque, A. K. M. M.; Kashem, M. A.; Lam, S. S.; Ong, H. C.; Uddin, M. A.; Mofijur, M. Prospect of Biobased Antiviral Face Mask to Limit the Coronavirus Outbreak. *Environ. Res.* **2021**, *192*, No. 110294.
- (22) Geetha, K.; Sivasangari, D.; Kim, H.-S.; Murugadoss, G.; Kathalingam, A. Electrospun Nanofibrous ZnO/PVA/PVP Composite Films for Efficient Antimicrobial Face Masks. *Ceram. Int.* **2022**, 48, 29197–29204.
- (23) Sugumaran, K. R.; Ponnusami, V. Review on Production, Downstream Processing and Characterization of Microbial Pullulan. *Carbohydr. Polym.* **2017**, *173*, 573–591.
- (24) Singh, R. S.; Kaur, N.; Rana, V.; Kennedy, J. F. Pullulan: A Novel Molecule for Biomedical Applications. *Carbohydr. Polym.* **2017**, 171, 102–121.
- (25) Hsiung, E.; Celebioglu, A.; Kilic, M. E.; Durgun, E.; Uyar, T. Fast-Disintegrating Nanofibrous Web of Pullulan/Griseofulvin—Cyclodextrin Inclusion Complexes. *Mol. Pharmaceutics* **2023**, 20, 2624–2633.
- (26) Hsiung, E.; Celebioglu, A.; Chowdhury, R.; Kilic, M. E.; Durgun, E.; Altier, C.; Uyar, T. Antibacterial Nanofibers of Pullulan/Tetracycline-Cyclodextrin Inclusion Complexes for Fast-Disintegrating Oral Drug Delivery. *J. Colloid Interface Sci.* **2022**, *610*, 321–333.
- (27) Celebioglu, A.; Uyar, T. Electrohydrodynamic Encapsulation of Eugenol-Cyclodextrin Complexes in Pullulan Nanofibers. *Food Hydrocolloids* **2021**, *111*, No. 106264.
- (28) Hou, T.; Sana, S. S.; Li, H.; Xing, Y.; Nanda, A.; Netala, V. R.; Zhang, Z. Essential Oils and Its Antibacterial, Antifungal and Anti-Oxidant Activity Applications: A Review. *Food Biosci.* **2022**, *47*, No. 101716
- (29) Doyle, A. A.; Stephens, J. C. A Review of Cinnamaldehyde and Its Derivatives as Antibacterial Agents. *Fitoterapia* **2019**, *139*, No. 104405.
- (30) Kayaci, F.; Ertas, Y.; Uyar, T. Enhanced Thermal Stability of Eugenol by Cyclodextrin Inclusion Complex Encapsulated in Electrospun Polymeric Nanofibers. *J. Agric. Food Chem.* **2013**, *61*, 8156–8165.
- (31) Kayaci, F.; Sen, H. S.; Durgun, E.; Uyar, T. Functional Electrospun Polymeric Nanofibers Incorporating Geraniol-Cyclo-

- dextrin Inclusion Complexes: High Thermal Stability and Enhanced Durability of Geraniol. *Food Res. Int.* **2014**, *62*, 424–431.
- (32) Paiva-Santos, A. C.; Ferreira, L.; Peixoto, D.; Silva, F.; Soares, M. J.; Zeinali, M.; Zafar, H.; Mascarenhas-Melo, F.; Raza, F.; Mazzola, P. G.; Veiga, F. Cyclodextrins as an Encapsulation Molecular Strategy for Volatile Organic Compounds—Pharmaceutical Applications. *Colloids Surf., B* **2022**, *218*, No. 112758.
- (33) Crini, G. A History of Cyclodextrins. Chem. Rev. 2014, 114, 10940-10975.
- (34) Yildiz, Z. I.; Kilic, M. E.; Durgun, E.; Uyar, T. Molecular Encapsulation of Cinnamaldehyde within Cyclodextrin Inclusion Complex Electrospun Nanofibers: Fast-Dissolution, Enhanced Water Solubility, High Temperature Stability and Antibacterial Activity of Cinnamaldehyde. *J. Agric. Food Chem.* **2019**, *67*, 11066–11076.
- (35) Hedayati, N.; Montazer, M.; Mahmoudirad, M.; Toliyat, T. Ketoconazole and Ketoconazole/ $\beta$ -Cyclodextrin Performance on Cotton Wound Dressing as Fungal Skin Treatment. *Carbohydr. Polym.* **2020**, 240, No. 116267.
- (36) Hedayati, N.; Montazer, M.; Mahmoudirad, M.; Toliyat, T. Cotton Fabric Incorporated with  $\beta$ -Cyclodextrin/Ketoconazole/Ag NPs Generating Outstanding Antifungal and Antibacterial Performances. *Cellulose* **2021**, 28, 8095–8113.
- (37) Li, D.; Frey, M. W.; Joo, Y. L. Characterization of Nanofibrous Membranes with Capillary Flow Porometry. *J. Membr. Sci.* **2006**, *286*, 104–114.
- (38) Xiao, M.; González, E.; Monterroza, A. M.; Frey, M. Fabrication of Thermo-Responsive Cotton Fabrics Using Poly (Vinyl Caprolactam-Co-Hydroxyethyl Acrylamide) Copolymer. *Carbohydr. Polym.* **2017**, *174*, 626–632.
- (39) Zangmeister, C. D.; Radney, J. G.; Staymates, M. E.; Vicenzi, E. P.; Weaver, J. L. Hydration of Hydrophilic Cloth Face Masks Enhances the Filtration of Nanoparticles. *ACS Appl. Nano Mater.* **2021**, *4*, 2694–2701.
- (40) Mittal, R.; Meneveau, C.; Wu, W. A Mathematical Framework for Estimating Risk of Airborne Transmission of COVID-19 with Application to Face Mask Use and Social Distancing. *Phys. Fluids* **2020**, *32*, No. 101903.
- (41) Angeles, M.; Cheng, H.; Velankar, S. S. Emulsion Electrospinning: Composite Fibers from Drop Breakup during Electrospinning. *Polym. Adv. Technol.* **2008**, *19*, 728–733.
- (42) García-Moreno, P. J.; Stephansen, K.; van der Kruijs, J.; Guadix, A.; Guadix, E. M.; Chronakis, I. S.; Jacobsen, C. Encapsulation of Fish Oil in Nanofibers by Emulsion Electrospinning: Physical Characterization and Oxidative Stability. *J. Food Eng.* **2016**, *183*, 39–49.
- (43) Uyar, T.; Besenbacher, F. Electrospinning of Uniform Polystyrene Fibers: The Effect of Solvent Conductivity. *Polymer* **2008**, *49*, 5336–5343.
- (44) Babaahmadi, V.; Amid, H.; Naeimirad, M.; Ramakrishna, S. Biodegradable and Multifunctional Surgical Face Masks: A Brief Review on Demands during COVID-19 Pandemic, Recent Developments, and Future Perspectives. *Sci. Total Environ.* **2021**, 798, No. 149233.
- (45) Pandit, P.; Maity, S.; Singha, K.; Uzun, M.; Shekh, M.; Ahmed, S. Potential Biodegradable Face Mask to Counter Environmental Impact of Covid-19. *Clean. Eng. Technol.* **2021**, *4*, No. 100218.
- (46) Deng, Y.; Lu, T.; Zhang, X.; Zeng, Z.; Tao, R.; Qu, Q.; Zhang, Y.; Zhu, M.; Xiong, R.; Huang, C. Multi-Hierarchical Nanofiber Membrane with Typical Curved-Ribbon Structure Fabricated by Green Electrospinning for Efficient, Breathable and Sustainable Air Filtration. J. Membr. Sci. 2022, 660, No. 120857.
- (47) Mazrouei-Sebdani, Z.; Khoddami, A.; Hadadzadeh, H.; Zarrebini, M.; Karimi, A.; Shams-Ghahfarokhi, F. The Effect of the Nano-Structured Aerogel Powder on the Structural Parameters, Water Repellency, and Water Vapor/Air Permeability of a Fibrous Polyester Material. *Mater. Chem. Phys.* **2016**, *177*, 99–111.
- (48) Zhao, J.; Zhu, W.; Wang, X.; Liu, L.; Yu, J.; Ding, B. Fluorine-Free Waterborne Coating for Environmentally Friendly, Robustly Water-Resistant, and Highly Breathable Fibrous Textiles. *ACS Nano* **2019**, *14*, 1045–1054.

- (49) Zhou, W.; Gong, X.; Li, Y.; Si, Y.; Zhang, S.; Yu, J.; Ding, B. Environmentally Friendly Waterborne Polyurethane Nanofibrous Membranes by Emulsion Electrospinning for Waterproof and Breathable Textiles. *Chem. Eng. J.* **2022**, 427, No. 130925.
- (50) Ullah, S.; Ullah, A.; Lee, J.; Jeong, Y.; Hashmi, M.; Zhu, C.; Joo, K.; Cha, H. J.; Kim, I. S. Reusability Comparison of Melt-Blown vs Nanofiber Face Mask Filters for Use in the Coronavirus Pandemic. *ACS Appl. Nano Mater.* **2020**, *3*, 7231–7241.
- (51) Zhou, W.; Gong, X.; Li, Y.; Si, Y.; Zhang, S.; Yu, J.; Ding, B. Waterborne Electrospinning of Fluorine-Free Stretchable Nanofiber Membranes with Waterproof and Breathable Capabilities for Protective Textiles. *J. Colloid Interface Sci.* 2021, 602, 105–114.
- (52) Abuzade, R. A.; Zadhoush, A.; Gharehaghaji, A. A. Air Permeability of Electrospun Polyacrylonitrile Nanoweb. *J. Appl. Polym. Sci.* **2012**, *126*, 232–243.
- (53) Celebioglu, A.; Ipek, S.; Durgun, E.; Uyar, T. Selective and Efficient Removal of Volatile Organic Compounds by Channel-Type Gamma-Cyclodextrin Assembly through Inclusion Complexation. *Ind. Eng. Chem. Res.* **2017**, *56*, 7345–7354.
- (54) Seethu, B. G.; Pushpadass, H. A.; Emerald, F. M. E.; Nath, B. S.; Naik, N. L.; Subramanian, K. S. Electrohydrodynamic Encapsulation of Resveratrol Using Food-Grade Nanofibres: Process Optimization, Characterization and Fortification. *Food Bioprocess Technol.* **2020**, *13*, 341–354.
- (55) Tian, Y.; Yuan, C.; Cui, B.; Lu, L.; Zhao, M.; Liu, P.; Wu, Z.; Li, J. Pickering Emulsions Stabilized by  $\beta$ -Cyclodextrin and Cinnamaldehyde Essential Oil/ $\beta$ -Cyclodextrin Composite: A Comparison Study. *Food Chem.* **2022**, *377*, No. 131995.
- (56) Liu, F.; Türker Saricaoglu, F.; Avena-Bustillos, R. J.; Bridges, D. F.; Takeoka, G. R.; Wu, V. C. H.; Chiou, B.-S.; Wood, D. F.; McHugh, T. H.; Zhong, F. Preparation of Fish Skin Gelatin-Based Nanofibers Incorporating Cinnamaldehyde by Solution Blow Spinning. *Int. J. Mol. Sci.* **2018**, *19*, 618.
- (57) Yang, Y.; Xie, B.; Liu, Q.; Kong, B.; Wang, H. Fabrication and Characterization of a Novel Polysaccharide Based Composite Nanofiber Films with Tunable Physical Properties. *Carbohydr. Polym.* **2020**, 236, No. 116054.
- (\$8) Shao, P.; Niu, B.; Chen, H.; Sun, P. Fabrication and Characterization of Tea Polyphenols Loaded Pullulan-CMC Electrospun Nanofiber for Fruit Preservation. *Int. J. Biol. Macromol.* **2018**, 107, 1908–1914.
- (59) Mura, P. Analytical Techniques for Characterization of Cyclodextrin Complexes in the Solid State: A Review. *J. Pharm. Biomed. Anal.* **2015**, *113*, 226–238.
- (60) Wadhwa, G.; Kumar, S.; Chhabra, L.; Mahant, S.; Rao, R. Essential Oil-Cyclodextrin Complexes: An Updated Review. *J. Inclusion Phenom. Macrocyclic Chem.* **2017**, 89, 39–58.
- (61) Kowalczyk, D.; Skrzypek, T.; Basiura-Cembala, M.; Łupina, K.; Mzyńska, M. The Effect of Potassium Sorbate on the Physicochemical Properties of Edible Films Based on Pullulan, Gelatin and Their Blends. *Food Hydrocolloids* **2020**, *105*, No. 105837.
- (62) Neacşu, A. Physicochemical Investigation of the Complexation between  $\gamma$ -Cyclodextrin and Doxorubicin in Solution and in Solid State. *Thermochim. Acta* **2018**, *661*, 51–58.
- (63) Aydogdu, A.; Yildiz, E.; Aydogdu, Y.; Sumnu, G.; Sahin, S.; Ayhan, Z. Enhancing Oxidative Stability of Walnuts by Using Gallic Acid Loaded Lentil Flour Based Electrospun Nanofibers as Active Packaging Material. *Food Hydrocolloids* **2019**, *95*, 245–255.
- (64) Ertan, K.; Celebioglu, A.; Chowdhury, R.; Sumnu, G.; Sahin, S.; Altier, C.; Uyar, T. Carvacrol/Cyclodextrin Inclusion Complex Loaded Gelatin/Pullulan Nanofibers for Active Food Packaging Applications. *Food Hydrocolloids* **2023**, *142*, No. 108864.
- (65) Herrera, A.; Rodríguez, F. J.; Bruna, J. E.; Abarca, R. L.; Galotto, M. J.; Guarda, A.; Mascayano, C.; Sandoval-Yáñez, C.; Padula, M.; Felipe, F. R. S. Antifungal and Physicochemical Properties of Inclusion Complexes Based on  $\beta$ -Cyclodextrin and Essential Oil Derivatives. *Food Res. Int.* **2019**, *121*, 127–135.
- (66) Zhou, Z.; Liu, Y.; Liu, Z.; Fan, L.; Dong, T.; Jin, Y.; Saldaña, M. D. A.; Sun, W. Sustained-Release Antibacterial Pads Based on

- Nonwovens Polyethylene Terephthalate Modified by  $\beta$ -Cyclodextrin Embedded with Cinnamaldehyde for Cold Fresh Pork Preservation. *Food Packag. Shelf Life* **2020**, *26*, No. 100554.
- (67) Shruthi, T. S.; Meghana, M. R.; Medha, M. U.; Sanjana, S.; Navya, P. N.; Daima, H. K. Streptomycin Functionalization on Silver Nanoparticles for Improved Antibacterial Activity. *Mater. Today Proc.* **2019**, *10*, 8–15.
- (68) Yang, Y.; Zheng, S.; Liu, Q.; Kong, B.; Wang, H. Fabrication and Characterization of Cinnamaldehyde Loaded Polysaccharide Composite Nanofiber Film as Potential Antimicrobial Packaging Material. Food Packag. Shelf Life 2020, 26, No. 100600.
- (69) Teixeira, M. A.; Antunes, J. C.; Seabra, C. L.; Fertuzinhos, A.; Tohidi, S. D.; Reis, S.; Amorim, M. T. P.; Ferreira, D. P.; Felgueiras, H. P. Antibacterial and Hemostatic Capacities of Cellulose Nanocrystalline-Reinforced Poly (Vinyl Alcohol) Electrospun Mats Doped with Tiger 17 and Pexiganan Peptides for Prospective Wound Healing Applications. *Biomater. Adv.* 2022, 137, No. 212830.
- (70) Li, Y.; Hua, Y.; Ji, Z.; Wu, Z.; Fan, J.; Liu, Y. Dual-Bionic Nano-Groove Structured Nanofibers for Breathable and Moisture-Wicking Protective Respirators. *J. Membr. Sci.* **2023**, *672*, No. 121257.

# **□** Recommended by ACS

Microfluidic Spinning of Metal-Organic Framework-Loaded Nanofibers toward High-Efficient Particulate Matter Removal and Antibacterial Filters

Ting Dong, Su Chen, et al.

SEPTEMBER 15, 2023

INDUSTRIAL & ENGINEERING CHEMISTRY RESEARCH

READ 🗹

Electrospray-on-Electrospun Breathable, Biodegradable, and Robust Nanofibrous Membranes with Photocatalytic Bactericidal Activity

Qi Feng Lim, Junhua Kong, et al.

JANUARY 19, 2023

ACS APPLIED NANO MATERIALS

READ 🗹

# Reusable Electrospun Nanofibrous Membranes with Antibacterial Activity for Air Filtration

Guangyao Wang, Junwei Ye, et al.

JUNE 02, 2023

ACS APPLIED NANO MATERIALS

READ 🗹

## Photothermal Electrospun Nanofibers Containing Polydopamine-Coated Halloysite Nanotubes as Antibacterial Air Filters

Oyku Demirel, Hayriye Unal, et al.

NOVEMBER 23, 2022

ACS APPLIED NANO MATERIALS

READ 🗹

Get More Suggestions >